The Role of Surface States in the Ultrafast Photoinduced Electron Transfer from Sensitizing Dye Molecules to Semiconductor Colloids

Robert Huber,[†] Sebastian Spörlein,[†] Jacques E. Moser,[‡] Michael Grätzel,[‡] and Josef Wachtveitl*,[†]

Lehrstuhl für BioMolekulare Optik, Oettingenstrasse 67, Ludwig-Maximilians-Universität München, 80538 München, Germany, Laboratory for Photonics & Interfaces, Department of Chemistry, Ecole Polytechnique Fédérale de Lausanne, CH-1015 Lausanne, Switzerland

Received: December 20, 1999; In Final Form: April 13, 2000

Investigations on the ultrafast electron injection mechanism from the dye alizarin to wide band gap semiconductor colloids in aqueous medium are presented, combined with detailed studies on population, depopulation, and relaxation phenomena in trap states and their influence on the injection process. Because of the very strong electronic coupling between dye and semiconductor in an alizarin/TiO_2 system, a very fast electron injection from the excited dye to the conduction band of TiO_2 is expected. Our measurements show an injection time $\tau_{inj} < 100$ fs, suggesting that the electron transfer follows an adiabatic mechanism. Furthermore, we present experiments over a wide spectral range on the recombination reaction of the electron in the conduction band of the semiconductor colloid and the dye cation to the ground state. We find highly multiphasic recombination dynamics with time constants from 400 fs to the nanosecond time scale. The nonexponential character of the recombination reaction is attributed to fast relaxation processes. The crucial contribution of surface trap states and their influence on the observed dynamics was investigated with alizarin adsorbed on the insulating substrate ZrO_2. Since the conduction band edge lies far above ($\approx$1 eV) the S_1 state of alizarin, the electron injection into this band is completely suppressed. Despite this fact our spectroscopic investigations show that on ultrafast time scales the formation of an alizarin cation occurs. This observation, is explained by fast electron injection into surface trap states near the docking site on the colloid. For the alizarin/ZrO_2 system the time scale for the injection into these traps is determined to be faster than 100 fs. The relaxation processes in the traps and the repopulation of the S_1 state occur within 450 fs, the subsequent ground-state relaxation takes 160 ps. The ultrafast injection dynamics into the traps, recorded for alizarin/ZrO_2, underlines the importance of surface states for the initial charge separation also for systems with a lower band edge such as TiO_2. We show that in the dye/ZrO_2 system the process of electron injection is not suppressed but "stopped" after the ultrafast transition into trap states. It is therefore a valuable system for probing the electron dynamics in surface states.

I. Introduction

Sensitization of wide band gap semiconductors by organic dye molecules has attracted much interest during the last years. Recently suggested and partially already realized applications such as the decontamination of water[1] or the efficient conversion of solar energy to electricity provide some of the driving forces in the effort for a better understanding of the underlying processes.[2−5] The basic photophysical reactions can be written as

$$S + h\nu \rightarrow S^* \rightarrow S^+ + e^-_{CB}(TiO_2)$$

The dye (S) is excited with visible light ($h\nu$) to the electronically excited state S*. If this state lies energetically above the conduction band edge of the colloid, electron injection to the semiconductor can occur on a fast or ultrafast time scale.[6−23] The resulting charge-separated system was reported to undergo relaxation and recombination processes, with typical time constants in the range from 10 fs up to 500 μs,[9,12,21,24,25] dependent on the dye/semiconductor system. According to Marcus theory one of the main parameters for the electron injection rate is the difference in free energy ΔG between the donor and acceptor states. Thus, the energetic position of the acceptor level plays a key role for the dynamics of the injection mechanism. Up to now only the high density (conduction band continuum) of acceptor states was regarded as the main reason for the ultrafast initial charge separation. The role of surface states as possible primary acceptors cannot be investigated in detail in systems such as TiO_2, where the electron is immediately injected into the conduction band. Higher band gap semiconductor colloids such as ZrO_2 may serve as an ideal system to investigate the role of these surface states, since a further transfer of the electron is impossible. Trap states at the colloidal surface are caused by the nonisotropic environment provoked by the perturbed crystal structure at the surface, the coupled dye, or the solvent.

The electronic coupling V is another major factor determining the electron transfer kinetics. The overlap of the electronic wave functions of donor and acceptor critically depend on the spatial arrangement of the system. Selection of adequate dyes allows an easy systematic variation of V in the dye colloidal system.

[†] Ludwig-Maximilians-Universität München. E-mail for J.W.: Josef.Wachtveitl@physik.uni-muenchen.de.

[‡] Ecole Polytechnique Fédérale de Lausanne. E-mail for J.E.M.: JE.Moser@epfl.ch.

10.1021/jp9944381 CCC: $19.00
Published on Web 09/06/2000

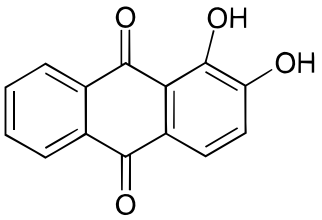

Figure 1. Chemical structure of alizarin, the sensitizing dye.

Recently, various studies on the reaction dynamics of dye/semiconductor colloid systems with moderate electronic coupling strength were performed.[6,15−18] Here we report the dynamics of electron injection and recombination of alizarin/TiO_2, a system with a considerably higher electronic coupling for charge injection.[25,40] Figure 1 presents the chemical structure of the dye alizarin with the two chelating hydroxyl groups coupling the dye to the surface titanium/zirconium ions of the semiconductor colloid.

II. Experimental Section

Measurements were performed on three different samples: alizarin, alizarin coupled to TiO_2 colloids, and alizarin coupled to ZrO_2 colloids. The coupled systems were diluted in acidic water (pH < 3; 1 mM alizarin; 10 mg/mL TiO_2) or in methanol; the free dye (l mM) was diluted only in methanol. Colloidal nanoparticles of TiO_2 were prepared as previously described via hydrolysis of $TiCl_4$ in cold water and further dialysis of the sol.[38] No stabilizing polymer was used. The average diameter of oxide particles was about 16 nm, as measured by dynamic light scattering.

ZrO_2 colloidal dispersions were prepared by hydrolysis of zirconium chloride in methanol. $ZrCl_4$ powder (10 g) (Alfa) was dissolved in 150 mL of absolute methanol. The solution was cooled to 0 °C, acidified by 0.5 mL concentrated HCl, and 4 mL of H_2O was added. After 2 h of stirring at room temperature, the colloid was boiled under reflux for 2−3 h. The concentrated methanolic solution (150 mL) was finally diluted in pure water (700 mL) to yield a transparent colloid containing typically 6 g/L ZrO_2 particles and ca. 18 vol % methanol. The hydrodynamic diameter of the ZrO_2 colloidal particles determined by quasi-elastic light scattering was 10−20 nm.

The dye adsorption process in aqueous solution was performed by adding the solid dye to the aqueous colloids under continuous stirring. Because alizarin is not soluble in pure water, the solvation process supports the coupling of the added alizarin to the surface of the semiconductor colloids. A similar procedure was carried out by presolving the alizarin in methanol and then adding the dissolved dye into the aqueous colloidal solution. This procedure resulted in identical spectral characteristics of this "presolved" sample in comparison to the one where solid alizarin was added.

For the samples in pure methanol, alizarin was also presolved and slowly added under continuous stirring to occupy homogeneously the available sites on the semiconductor surface of each colloid. The efficiency of the coupling process for the dye/TiO_2 samples was checked by fluorescence measurements observing the adsorption induced fluorescence quenching.

A first characterization of the investigated systems was performed by steady-state absorption and fluorescence measurements, recorded with commercial spectrometers, Perkin-Elmer (type Lambda 19) and a Spex fluorometer (type Fluorolog 2). The fluorescence spectra shown in Figure 3b were corrected for the absorption probability at the respective excitation wavelength.

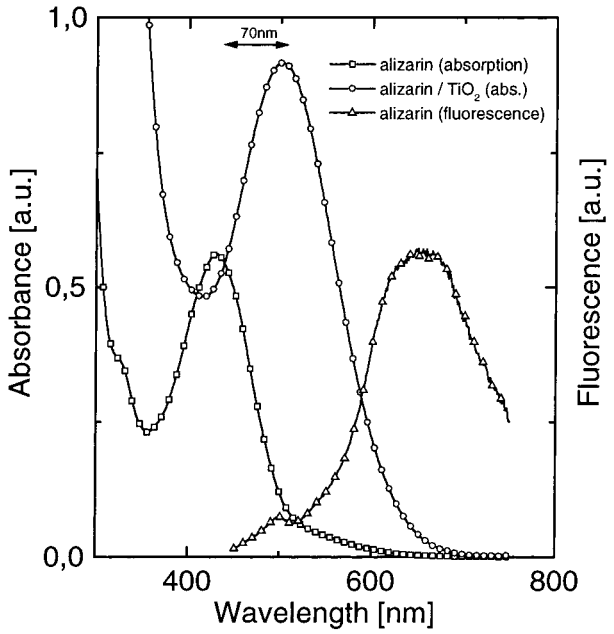

Figure 2. Absorption spectra of the free dye alizarin in methanol (squares) and of the coupled alizarin/TiO_2 system (circles) and fluorescence spectrum of the uncoupled alizarin (triangles). For the alizarin/ZrO_2 system an absorption spectrum almost identical to that for alizarin/TiO_2 (not shown) was measured. The large shift of the main absorption band of about 70 nm due to the coupling process reflects the high electronic coupling constant. The charge-transfer character of the new band is expressed by an increased extinction coefficient of the coupled systems.

For the femtosecond time-resolved transient absorption measurements by the pump−probe technique we used a home-built 20 Hz Ti:sapphire laser system with a pulse width of about 100 fs (fwhm) and a pulse energy of 600 μJ at a central wavelength of 870 nm.[26a] The main part of the 870 nm output was frequency doubled and either directly used for the excitation of the sample at 435 nm or for pumping a noncollinear optical parametric amplifier (NOPA) with a tunable wavelength ranging from 490 to 750 nm. The setup is described in detail in ref 27. The output pulses of the NOPA were compressed down to a duration of less than 50 fs (fwhm) at the excitation wavelength of 529 nm. Additionally, a white light continuum used for probing was generated from pulses (central wavelength 870 nm, energy 1 μJ) focused into a 2 mm sapphire plate. For the detection we used two separate spectrometers each with a 42 segment diode array ($\Delta\lambda = 8$ nm).[26b] The signal spectrometer recorded the actual transmission at a certain delay time t_D between pump and probe pulse, the reference spectrometer recorded simultaneously the spectrally resolved white light intensity. Every fifth pump pulse was blocked in order to recalibrate the recorded transmission by checking the ratio between the probe and the reference signals for the nonexcited sample. With these data the absorbance change for each delay time can be calculated to avoid long-term drift effects. These are caused by the diodes and their respective amplifiers as well as by slightly varying spatial distributions of the white light probing continuum, which would result in a drift in the zero absorption change.

The signals from the diode arrays were recorded by a multichannel a/d converter connected to a PC operating in single shot detection mode. The cross correlation time between the pump pulse and the white light probe was about 140 fs for the 435 nm pump pulses (generated by frequency doubling the output of the 20 Hz Ti:sapphire regenerative amplifier) and 80

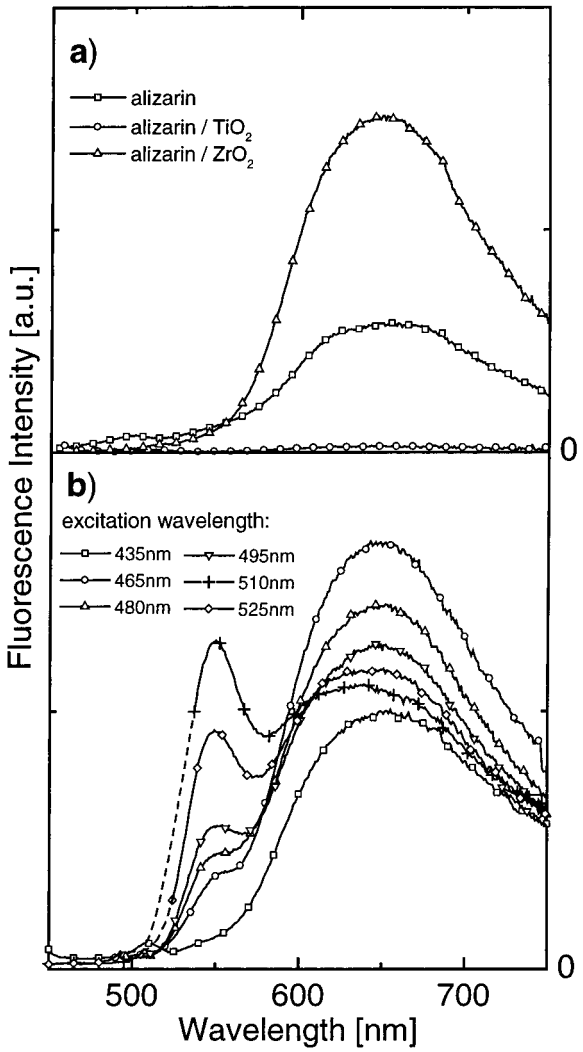

Figure 3. (a) Fluorescence spectra of free uncoupled alizarin (squares), alizarin/TiO_2 (circles), and alizarin/ZrO_2 (triangles). The effective electron injection into TiO_2 leads to a totally quenched fluorescence, whereas for the ZrO_2 system an even increased emission can be measured. The absence of flourescence in the case of TiO_2 also indicates a high ratio of coupled to uncoupled molecules. (b) Excitation dependence of alizarin/ZrO_2 fluorescence. The data in the Rayleigh scattering regions are omitted, and the undisturbed areas in the spectra are connected by a spline curve (dashed). The occurrence of two emission maxima can be explained by two different emitting electronic states—e.g., the excited state of the alizarin and a trap state at the colloidal surface. The fluorescence band at longer wavelengths ($\lambda >$ 600 nm) increases with decreasing excitation wavelengths.

fs for the 529 nm pump pulses (generated with the NOPA). The experimental delay time zero position and the instrumental response function for each channel were determined by recording the temporal evolution of the dye fluorol 6G (Lambda Physik) in ethanol.

The transient absorption kinetics were fitted by a global fitting algorithm allowing us to minimize the least mean square for all 42 recorded transients with n global decay times and $42 \times n$ local linear parameters at once, taking into account the experimentally determined cross correlation functions for each channel.

Molecular orbitals, optimized geometries, and electronic spectra for free and adsorbed dye molecules were calculated using the Tektronix CAChe molecular mechanics program package. Geometrical optimizations were performed using MOPAC (AM1 parameter set) for the free alizarin dye and ZINDO for the alizarin Ti(IV) complex (INDO/1 parameter set). In both cases SCF and CI calculations were then carried out with ZINDO (10 configuration interactions) to calculate electronic transition energies and intensities. The aqueous environment was simulated during SCF.

III. Results

Steady-State Spectroscopy, MO Calculations. The steady-state spectra in Figure 2 show the absorption of free alizarin in methanol and alizarin sensitized TiO_2 nanoparticles as well as the fluorescence of free alizarin. The strong shift of the absorption maximum of about 70 nm from 430 to 500 nm upon adsorption indicates a very large electronic coupling between alizarin and the semiconductor surface and the appearance of a new ligand-to-metal charge-transfer absorption band.[28]

In MO calculations we assume a linkage of alizarin through the two chelating −OH groups of its catechol moiety to one surface Ti^{4+} ion. This assumption is based on the experimental finding that complexation of the surface of titanium dioxide by alizarin follows a Langmuir type isotherm with a stability constant $K_L = 8 \times 10^4$ L mol^{-1}, identical to that obtained for adsorption of catechol in similar conditions.[39] As a result, these calculations are able to reproduce the changes of electronic properties of alizarin upon adsorption, namely a pronounced red shift of the absorption band and an increase of the extinction coefficient. Calculated HOMO and LUMO orbitals indicate that anchoring of alizarin onto the surface of TiO_2 leads to a new LMCT type $\pi-$d transition and, therefore, that the surface alizarin−Ti(IV) charge-transfer complex acts as the active chromophore in coupled systems upon irradiation at wavelengths between 450 and 650 nm.

From the values of the maximum molar extinction coefficient, ϵ_{max} ($\lambda = 500$ nm) $= 8.69 \times 10^3$ mol^{-1} L cm^{-1} of the Ti−alizarin complex, the CT band maximum $\bar{\nu}_{max} = 20\,110$ cm^{-1}, and band width $\Delta\bar{\nu}_{1/2} = 4754$ cm^{-1}, the oscillating strength and the transition dipole moment of the $\pi-$d transition are estimated to be $f = 0.28$ and $M = 5.4$ D, respectively. The electronic matrix element $|H|$ coupling a ground state to a charge-transfer excited state can be calculated from the energy and intensity of the charge-transfer transition using the Mulliken−Hush equation.[42] Using the spectroscopic quantities obtained from the absorption spectrum of the surface complex, and assuming a donor−acceptor separation $r_{DA} \cong 6$ Å, corresponding roughly to the distance between the center of the π system of alizarin to the chelated Ti^{4+} ion, a value of $|H_{DA}| = 3.1 \times 10^3$ cm^{-1} ($\cong 15\ kT$) is estimated that corresponds indeed to a very large electronic coupling.

From the Stokes shift of the free dye, an internal reorganization energy of 0.3 eV can be estimated, in agreement with previous calculations of the solvent reorganization energy for alizarin in ethanolic solution,[25] and experimental findings for other dyes.[6c] The weak sensitivity of the electronic properties of the alizarin/TiO_2 system to the medium (ethanolic vs aqueous solution; data not shown) further indicates the existence of a strong chelating interaction (see also refs 23 and 29).

In our study the alizarin/ZrO_2 system was originally intended to act as a reference system. Since the bottom of the conduction band for ZrO_2 is about 1.3 eV higher than for TiO_2—and therefore lies far above the $S_1(\nu = 0)$ energy level of the excited state of alizarin—no electron transfer from the dye to the semiconductor was expected in this case. The steady-state absorption properties, however, should be characteristic for a coupled system. The alizarin/ZrO_2 system indeed shows a pronounced shift of the absorption band (i.e., an alizarin/TiO_2

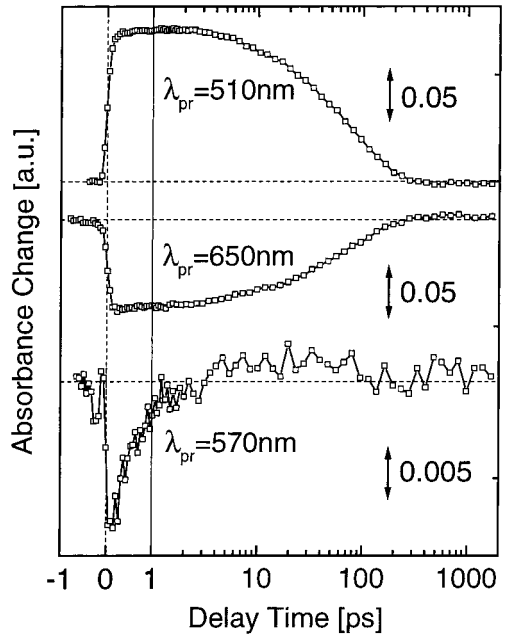

Figure 4. Three characteristic transients of free alizarin. The upper two curves compare transient signals caused by the excited-state absorption ($\lambda_{pr} = 510$ nm) and the stimulated emission ($\lambda_{pr} = 650$ nm). Both signals decay simultaneously with a typical time constant of 63 ps. In the spectral region where the two effects compensate each other ($\lambda_{pr} = 570$ nm) fast cooling processes of the excited dye can be observed with a very small amplitude.

like absorption spectrum) compared to the free dye. Furthermore, the fluorescence intensity of alizarin even increases upon adsorption at the ZrO_2 surface. This fact strongly supports the assumption of a nonreactive system. It is interesting to note that the fluorescence spectra of alizarin/ZrO_2 (Figure 3b) exhibit an unusual dependence on excitation wavelength: two fluorescence maxima at 550 and 650 nm can be observed. The emission band at 650 nm—also present in the fluorescence spectrum of free alizarin—dominates at short excitation wavelengths (e.g., $\lambda_{exc} = 435$ nm). An additional emission band appears around 550 nm; the strength of this band increases with increasing excitation wavelength.

Under the experimental conditions used, no fluorescence could be detected for the alizarin/TiO_2 system (Figure 3). Obviously, the fluorescence is completely quenched for alizarin/TiO_2 due to effective electron injection into the semiconductor, causing a fast depopulation of the S_1 state of alizarin. Therefore, the fluorescence measurements provide a very sensitive method to determine the ratio between TiO_2-coupled and uncoupled dye molecules.

Transient Measurements of Free Alizarin. Figure 4 shows three transients of alizarin in solution at different probing wavelengths (excitation centered around $\lambda_{exc} = 435$ nm). At a probing wavelength of $\lambda_{pr} = 510$ nm the transient absorbance change is dominated by an instantaneous increase in absorption due to the photoinduced formation of the excited state. A consecutive decrease of the signal to zero with a time constant of 63 ps reflects the recovery of the ground state. An absorbance change with opposite sign is observed in the spectral region between 610 and 700 nm, which is caused by stimulated emission. It decreases with the same time constant of 63 ps. So the temporal characteristics are dominated by the excited state decay dynamics of the dye. Only at $\lambda_{pr} = 570$ nm, where the strong signals from excited state absorption and stimulated emission compensate each other, small contributions from a faster process, presumably vibrational cooling within the excited

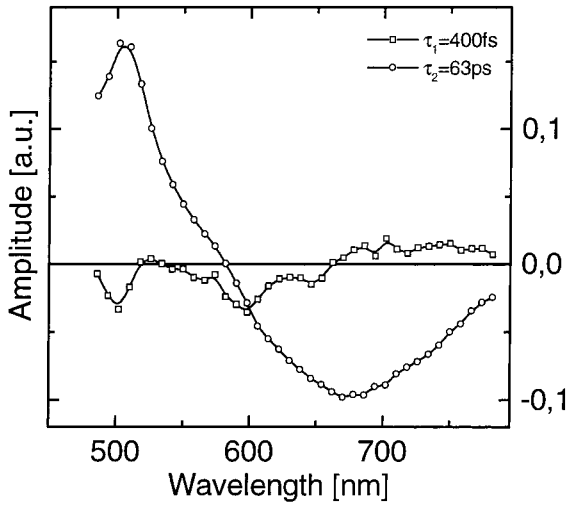

Figure 5. Decay associated spectra (amplitude spectra) of the recorded transients for free alizarin in methanol. The spectral characteristics of the 63 ps time constant—associated with the excited-state decay—indicates the location of the excited-state absorption (peak at 510 nm) and of the stimulated emission (peak at 670 nm).

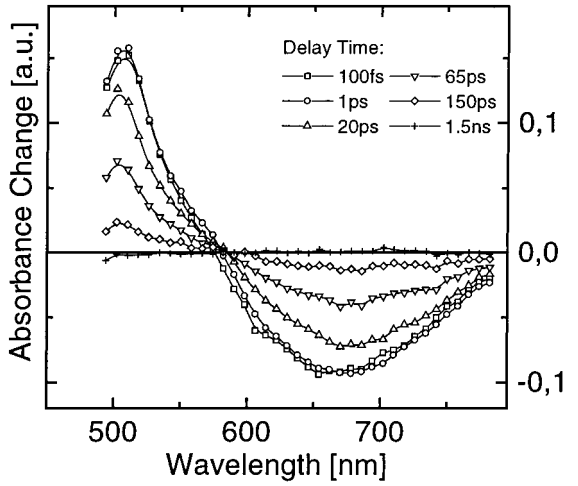

Figure 6. Transient absorption spectra of free alizarin at different delay times. The isosbestic point provides strong evidence for a monophasic relaxation.

electronic state of the dye can be observed with a typical time constant of 400 fs. The pronounced isosbestic point in the transient spectra (Figure 6) indicates that a two-state-reaction is observed. Figure 5 shows the decay associated spectra for the two time constants, which are sufficient for a good description of the complete set of experimental data: the amplitude of the 63 ps component exhibits maximal values at 510 and 670 nm and reflects the excited-state decay monitored by excited-state absorption and stimulated emission, respectively. The rather featureless spectral signature of the 400 fs time constant describes the wavelength dependence of the vibrational cooling.

Transient Measurements of Alizarin/TiO_2. Two typical transients for alizarin/TiO_2 excited at $\lambda_{exc} = 435$ nm and probed at $\lambda_{pr} = 502$ nm and $\lambda_{pr} = 742$ nm are shown in Figure 7. The temporal evolution of the transient absorbance changes for the alizarin/TiO_2 system is completely different compared to free alizarin. Most evident is the presence of an additional fast decrease of the initial signal amplitude, observed throughout the entire investigated spectral range. At $\lambda_{pr} = 502$ nm an instantaneous bleaching of the ground state can be observed, which decays with a marked fast component of 430 fs. The

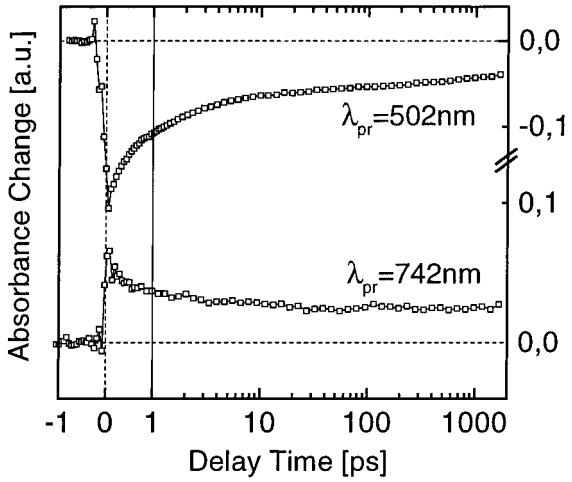

Figure 7. Transient absorbance kinetics for alizarin/TiO_2 measured at two different probing wavelengths. At $\lambda = 502$ nm the instantaneous bleaching and the incomplete recovery of the ground state can be observed.

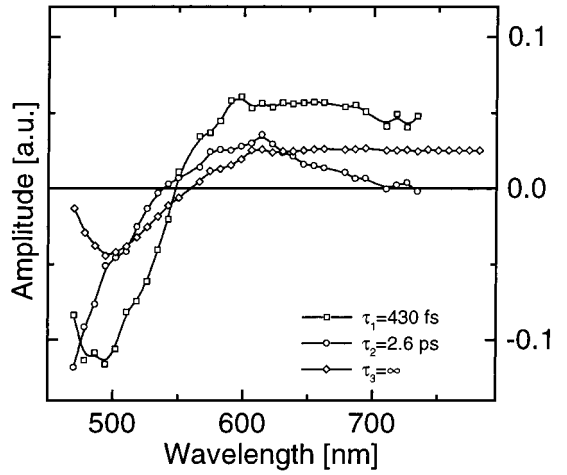

Figure 8. Amplitude spectra of alizarin/TiO_2. The residual signal ($\tau_3 = \infty$) between 450 and 550 nm reflects the decrease in ground-state absorption, the signal between 600 and 800 nm is due to absorption of injected electrons. Two additional time constants (15 ps, 390 ps) are used in the global fitting procedure. Since their amplitudes are very small (<0.015) throughout the entire investigated spectral range, they are omitted here.

remaining signal decreases continuously throughout the entire investigated temporal range. In contrast to the free dye, a residual signal remains at long delay times ($t_D > 1$ ns). This incomplete recovery of the ground state indicates the long persistence of a charge separated state after the photoinduced injection of an electron into the semiconductor. In the spectral region from 600 to 750 nm a new positive difference absorbance signal with a featureless spectral signature (Figures8 and 9) is observed. Several studies have shown that this contribution can be assigned to the absorption of the injected electron itself.[30−32] The temporal characteristics in this range are exemplified by the curve obtained at $\lambda_{pr} = 742$ nm (Figure 9, lower trace): the initial absorbance increase occurs within the experimental time resolution. The signal decreases very fast to a positive offset, which remains constant from 10 ps to 1 ns. The global fitting procedure of the transient signals shows that a satisfactory description can only be achieved by using at least five time constants. The spectral characteristics of the three main components are shown in Figure 8. However, it can be recognized in Figure 8 that the picosecond time constant contributes mainly at short probing

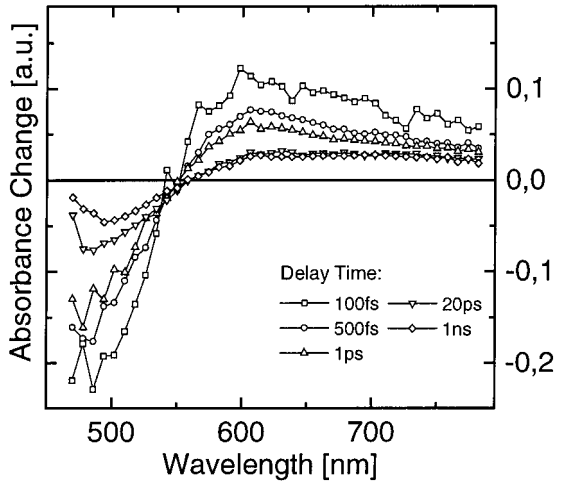

Figure 9. Transient absorption spectra of alizarin/TiO_2. There is no pronounced evolution in the spectral characteristics throughout the entire observed temporal range.

wavelengths ($\lambda_{pr} < 650$ nm). The temporal evolution of the conduction band electrons dominating the transient absorbance changes in the longer wavelengh region can be described with only two components (430 fs and infinity). The observed multiphasic dynamics can be caused by several consecutive reactions or by one highly nonexponential reaction. Inspection of the transient spectra again yields a pronounced isosbestic point (Figure 9). This lack of spectral evolution with increasing delay time t_D suggests that only one nonexponential reaction is observed in the time-resolved experiments. The transient absorbance changes at long delay times are clearly dominated by the contributions of the bleached ground state (around $\lambda_{pr} =$ 500 nm) and the absorption of the injected electron (for $\lambda_{pr} >$ 600 nm). Dynamics recorded with $\lambda_{exc} = 435$ nm and with $\lambda_{exc} = 529$ nm excitation showed almost the same temporal evolution (data not shown), indicating an identical reaction sequence for both sets of experiments.

Transient Measurements of Alizarin/ZrO_2. The three transients in Figure 10 of alizarin/ZrO_2 recorded at different probing wavelengths show additional dynamics, compared to the alizarin and the alizarin/TiO_2 systems. Within the first picosecond a fast component with a time constant of about 450 fs can be observed, similar to the one found in alizarin/TiO_2. In the plot for $\lambda_{pr} = 510$ nm an instantaneous bleaching of the ground-state absorption appears. It converts into a positive absorbance change after a few picoseconds and persists for more than 100 ps. Then the sign of the signal changes again and a negative long time offset for delay times $t_D > 2$ ns remains. This indicates an incomplete recovery of the alizarin/ZrO_2 ground state. The $\lambda_{pr} = 622$ nm curve shows a very similar kinetic behavior but an opposite sign compared to the transient at $\lambda_{pr} = 518$ nm. In the transient at $\lambda_{pr} = 726$ nm the same kinetic components can be found, with the difference of a missing ultrafast component $\tau < 1$ ps. An adequate description of the complete set of data is possible using the four time constants indicated in Figure 12. The main contributions are excited-state absorption (maximum at $\lambda_{pr} = 520$ nm) and emission signal (minimum at 680 nm), similar to the 63 ps component found for the free dye (Figure 5). Obviously, the amplitude spectra of the first and third component with time constants of $\tau_1 = 450$ fs and $\tau_2 = 160$ ps lie symmetric with respect to the $y = 0$ axis. This directly implies the population and the subsequent depopulation of an electronic state with a characteristic spectral signature.

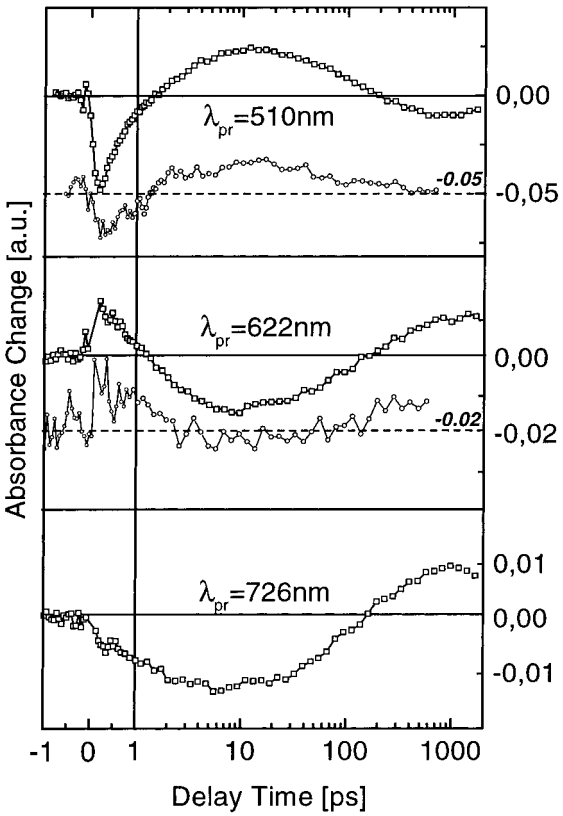

Figure 10. Transient absorption kinetics of alizarin/ZrO_2 at different probe wavelengths. The curves show a very complex dynamic behavior at spectral positions that should be dominated by ground- and excited-state absorption (λ_{pr} = 510 nm), emission (λ_{pr} = 622 and 726 nm), and electronic transitions within the colloid (λ_{pr} = 726 nm). Also in the alizarin/ZrO_2 system the ground state is not completely recovered within 2 ns. There are also two traces plotted, recorded with 529 nm excitation light, which show no characteristic differences (circles).

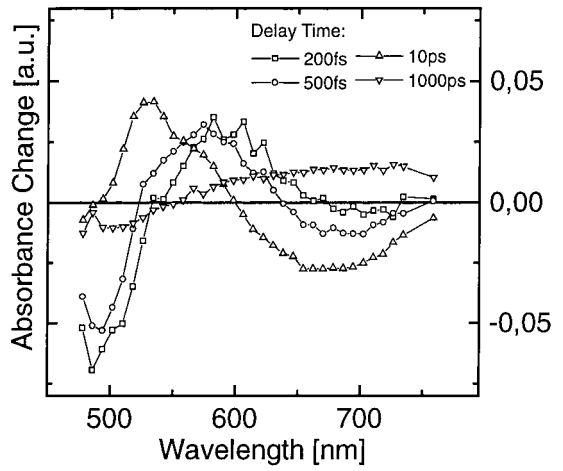

Figure 11. Transient spectra of alizarin/ZrO_2. The absence of an isosbestic point underlines the assumption that the temporal evolution of the spectral signature is not caused by simple ground-state relaxation but by multiphasic reaction dynamics.

The residual signal for delay times $t_D > 1$ ns is due to the existence of some long-lived species different from the alizarin ground state. The broad and featureless spectrum of the nanosecond transients is not characteristic for the dye molecule, but it is expected for electronic transitions within the semiconductor.

As mentioned above, the band gap of ZrO_2 is so high that hardly any electron acceptor levels are accessible for photo-

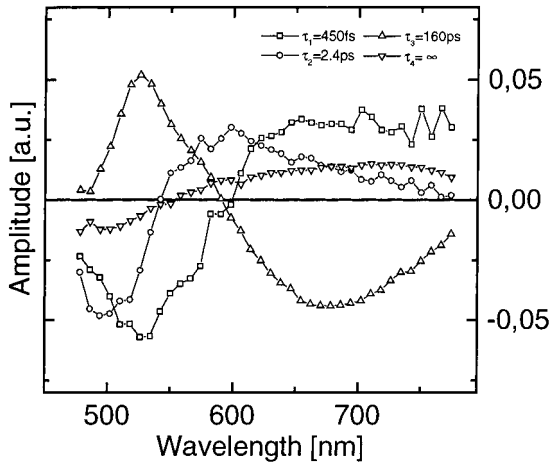

Figure 12. Amplitude spectra of alizarin/ZrO_2. The two spectra for the 450 fs and 160 ps decays lie symmetric to the $y = 0$ line and reflect the population and the consecutive depopulation of surface trap states in the ZrO_2.

excited alizarin. Therefore, the observation of highly multiphasic dynamics combined with the fact that no isosbestic point can be observed in the transient spectra (Figure 11) leads to the assumption that additional states have to be populated after excitation.

Analogous to the measurements on alizarin/TiO_2 there is no systematic discrepancy between excitation at λ_{exc} = 435 nm and λ_{exc} = 529 nm (Figure 10). The complex λ_{exc} = 529 nm transients certainly cannot be explained by a simple decay of the S_1 state of the photoexcited dye. Since the excitation energy was considerably lower in the λ_{exc} = 529 nm experiments, we can thus rule out the possibility that a two photon process leads to electron injection in the conduction band of ZrO_2. The implications will be discussed in detail below.

IV. Discussion

Singlet Excited State of Alizarin. The time-resolved evolution of the transient absorption spectrum of the investigated probe molecule is the most direct way to monitor the dynamics of this molecule. For alizarin in solution the lifetime of the excited singlet state can be determined by following the dynamics of the excited-state absorption or the stimulated emission. Both signals decay monoexponentially with a time constant of 63 ps. In selected spectral regions an additional fast component (τ = 400 fs) can be observed. The excited-state dynamics of the dye can be deduced from the femtosecond transients and the corresponding decay associated spectra (Figures 4−6): excitation of alizarin with a λ_{exc} = 435 nm pulse leads to a vibrationally hot state that thermalizes to the lowest vibrational level of the excited state within 400 fs and then decays to the ground state within 63 ps.

Interaction between Alizarin and TiO_2: Charge Separation. The energetics of the ground and excited state of alizarin is considerably affected upon its association with the colloidal surface.[25] Therefore, the efficiency of adsorption onto TiO_2 can be directly monitored via the electronic absorption and emission spectra. The quenching of the sensitizer fluorescence by the TiO_2 colloids is almost complete (Figure 3a), reflecting the high degree of association between the dye and TiO_2. The ZINDO calculations for alizarin/TiO_2 are able to reproduce the main features of the electronic transition and suggest that electron density is transferred to a considerable amount to the TiO_2 moiety. This has to be kept in mind when comparing the dynamic properties of the free and the associated alizarin.

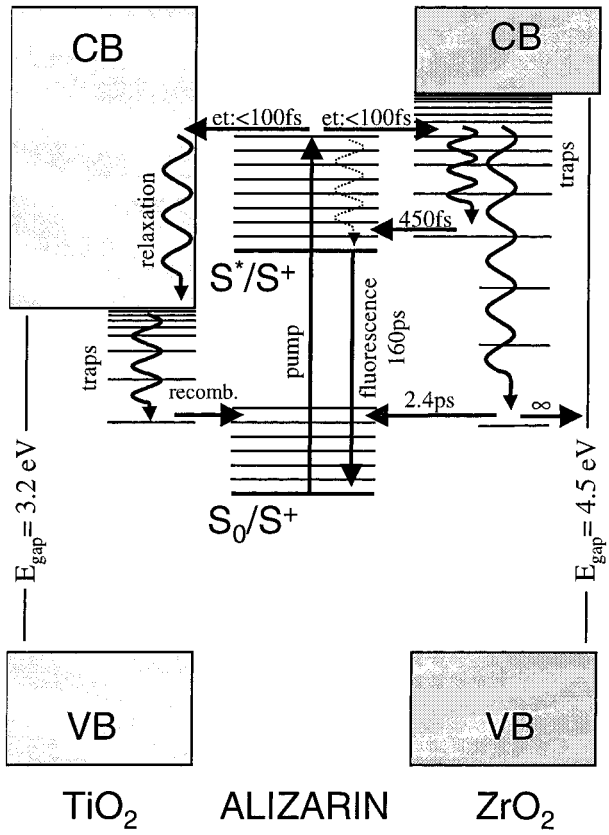

Figure 13. Energetic scheme for the coupled systems alizarin/TiO_2 (left) and alizarin/ZrO_2 (right). Relaxation processes are indicated by curved arrows, electronic transitions by straight ones. The arrow symbolized with ∞ marks the transition to remote traps forming long-lived charge separated states ($\tau > 1$ ns), which can be observed as residual signal in the time related spectra (Figure 12).

The energetic situation and a proposed mechanistic scheme for alizarin/TiO_2 are depicted in the diagram in Figure 13 (left). Here, the injection of an electron from the excited state of the dye directly into the conduction band of the semiconductor can occur. This interfacial electron transfer was studied for numerous dyes.[6−19,21,22,25,31−35] The fact that the charge injection process is usually much faster than the lifetime of the excited state of the dye is the prerequisite for the observed high quantum efficiency of the photochemical reaction. The long-time offset (which persists to delay times of $\tau > 1$ ns) of the transients for the alizarin/TiO_2 system (Figure 7) can be assigned to the slow recombination reaction of the long-lived charge separated state, which occurs on the microsecond time scale.[25] Therefore, this kinetics can be well distinguished from direct ground-state relaxation, which was determined to be 63 ps for the free alizarin (Figures 4−6).

In the shorter time domain, especially in the case of alizarin/TiO_2 with its high electronic coupling V, an ultrafast charge injection can be expected. In addition, for a high V value a strongly increased recombination rate for the electron in the conduction band and the dye cation to the ground state of alizarin should occur. As shown in Figure 13 three main reactions are triggered by an incident photon: (a) electron injection from the excited state of alizarin to the conduction band of the TiO_2 colloid, (b) relaxation/cooling processes of the hot electron in the conduction band and in trap states, and (c) recombination between the electron and alizarin cation. To assign these three reactions to the different features in the recorded transients, we consider the transient spectra (Figure 9). The pronounced isosbestic point at $\lambda_{pr} = 550$ nm indicates that only one of the three reactions mentioned above can be observed in our experimental data. The long-term characteristics of the spectra at $t_D = 1$ ns correlate well with the nanosecond measurements on the identical system published by Moser and Grätzel[25] and can therefore be assigned to the absorption of the charge separated state. Therefore, it can be concluded that the observed reaction kinetics throughout the entire investigated temporal range is dominated by the ground-state recombination. The electron injection as well as its relaxation in the conduction band is too fast to be observed with our present setup directly, despite a temporal resolution of typically 130 fs (cross correlation time) for the 435 nm excitation and 80 fs for the 529 nm excitation. However, these findings allow us to suggest an upper limit for the charge injection time of ≈100 fs for the system alizarin/TiO_2.

The observed multiphasic kinetics (Figure 8) for the alizarin/TiO_2 system reflects the highly nonexponential character of the ground-state recovery reaction. The nonexponential temporal evolution can be caused by diffusion processes in the colloid,[31,34−37] various kinds of surface traps, and multiple injection per colloid. These three effects are responsible for the wide temporal range of more than 8 orders of magnitude throughout which recombination reactions can be observed.[21,25] Global fitting procedures using a second-order decay function, as suggested by Hilgendorff et al.,[6c] did not result in good approximations of the experimental data in our system. The recombination pathway via repopulation of the S_1 state of alizarin is negligible, since TiO_2 trap states should energetically be well below the S_1 level of alizarin (Figure 13, left). This energetic situation is also reflected by the totally quenched fluorescence for TiO_2/alizarin (Figure 3a). The absence of any dominant systematic differences between excitation at 435 and 529 nm (data not shown) indicates similar reaction dynamics for the two cases (Figure 13 left) despite the excitation into different Franck−Condon regions of the S_1 potential energy surface.

Importance of Trap States: Alizarin/ZrO_2. ZrO_2 is supposed to be a good reference for dye semiconductor systems since it undergoes the same coupling process with the dye as TiO_2 but inhibits any electron injection into the conduction band due to its significantly higher band gap. The alizarin/TiO_2-like absorption spectrum of the alizarin/ZrO_2 system and its high fluorescence quantum yield observed in the steady-state emission experiments (Figure 3) support this view. The increase in fluorescence intensity for alizarin on ZrO_2 compared to alizarin in solution may be due to several reasons: alizarin in solution has a quite low fluorescence quantum yield. The dye molecules can dissipate their excitation energy via reversible proton transfer in a favorable six-membered transition state formed by internal H-bridging between the OH group in the 1-position and the anthraquinone function (see Figure 1). Upon adsorption on TiO_2 and ZrO_2 by surface chelation of metal cations, the hydroxyl groups of alizarin are deprotonated. Internal H-bonding mesomerism in this case is unfeasible and the nonradiative decay of the excited state less efficient. Furthermore, adsorption is also likely to rigidify the molecule and decrease the yield of internal conversion through low-frequency vibrational modes. The dye, if it were not quenched by electron transfer (as on TiO_2), would hence be expected to fluoresce much more strongly in the adsorbed state than in solution.

On the basis of the energetic situation and on the continuous wave (cw) experiments, it was therefore expected that the observed dynamics of the alizarin/ZrO_2 system reflects a simple ground-state recovery of the photoexcited coupled dye.[41]

However, the occurrence of fast reaction dynamics probed in the near-infrared has shown recently that in contrast to the expected nonreactivity also in dye/ZrO_2 systems electron transfer could take place, but so far no detailed investigations has addressed this point.[10] Figure 10 shows transients of the system alizarin/ZrO_2 excited at 435 nm that obviously show a highly multiphasic behavior with apparent time constants from $\tau =$ 450 fs to $\tau > 1$ ns (see also Figure 12). The temporal characteristics are totally different from that of free alizarin in solution. The absence of any isosbestic point in the transient spectra (Figure 11) indicates a more complex reaction scheme than for the dye or for the dye/TiO_2 samples. From the residual signal at $\tau > 1$ ns (Figure 11), which correlates almost perfectly with the data of alizarin/TiO_2 it can be deduced that also for alizarin/ZrO_2 at least a part of the excited molecules ends up in a long-lived charge separated state persisting for $\tau \gg 1$ ns.

In the following section the amplitude spectra are discussed for a detailed understanding of the processes following excitation of the alizarin/ZrO_2 sample (Figure 12). The various reactions are labeled with the assigned time constants in the schematic drawing (Figure 13, right). In a first approximation[1] this approach is exactly correct only for an unbranched reaction sequence with negligible back-reactions; each temporal component of the global fitting procedure characterizes the population/depopulation of an electronic state in the system. The spectral signature of the fitted amplitude for each component expresses the difference between the initial and final absorption spectra of the respective transition. The most obvious feature in the time related spectra is the symmetry of the 450 fs and the 160 ps component regarding the *x* axis. This is an evident sign for the population and the successive depopulation of a certain electronic state. The stimulated emission in the spectral region at $\lambda > 600$ nm (Figure 3) and the excited-state absorption around $\lambda_{max} = 520$ nm (slightly shifted due to ground-state bleaching; Figure 5) indicate the population of the "cold" S_1 state in 450 fs and its subsequent decay to the ground state within about 160 ps. The flat part of the 450 fs curve for $\lambda >$ 720 nm in Figure 12 represents a decreasing population of trapped electrons. This supports the assumption of an ultrafast recombination reaction between trapped electron and alizarin cation. Further evidence that the electron injection from alizarin to traps of ZrO_2 has already taken place within $\tau < 100$ fs (about the temporal resolution of our system) is given by the transient spectrum at 200 fs (Figure 11). The difference spectrum at $t_D = 200$ fs can be well identified as the contribution of the alizarin cation, which is supposed to have a similar spectrum as the alizarin cation coupled to TiO_2, shown in Figure 14. A small deviation between the difference spectrum in Figure 11 and the cation spectrum in Figure 14 for wavelengths $\lambda > 650$ nm is caused by the negative contribution of stimulated emission from the S_1 state and the absorption of the trapped electron. The signal for $\lambda < 600$ nm arises from the bleached ground-state absorption, which compensates the cation absorption at about 550 nm, in good agreement with the spectra in Figure 14. The amplitude spectrum of the 2.4 ps component (Figure 12) is characteristic for ground-state recombination between trapped electron and alizarin cation. At $\lambda_{pr} = 500$ nm the recovery of the ground-state absorption as well as the disappearance of the cation absorption can be seen. The decreasing signal at $\lambda_{pr} > 650$ nm can be ascribed to the weak electron absorption at long wavelengths if it is located in a deep trap after its relaxation. The residual signal in the transient spectra (Figure 12) is composed of a negative contribution due to nonrecovered ground state, cation absorption, and absorption of electrons in traps with weak electronic coupling to the alizarin molecule.

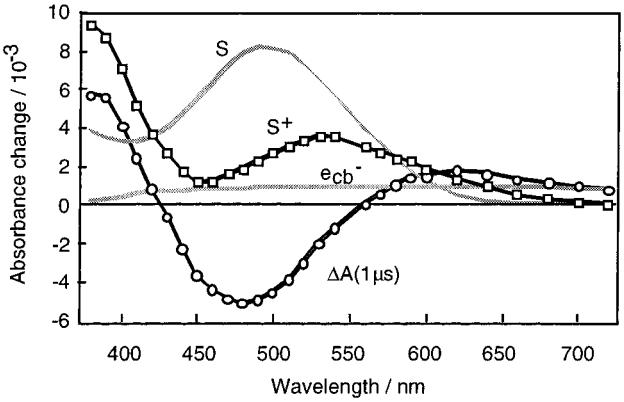

Figure 14. Spectra of alizarin/TiO_2, the alizarin cation and the electron in the conduction band, obtained by nanosecond transient measurements. ΔA (1 μs) is the transient difference spectrum after 1 μs. At 1 μs, the cation and the electron in the conduction band are the only absorbing species. If the cation spectrum is assumed to have a vanishing absorption at $\lambda = 720$ nm, it is possible to determine the contribution of the injected electron and also of the dye cation. The absorption of the oxidized species of alizarin coupled to ZrO_2 is assumed to be similar.

To resume the discussed scenario: after the excitation of the alizarin/ZrO_2 system, an electron is injected into surface trap states and cools therein with a time constant <100 fs. From the traps, one part of the electrons is reinjected in the lower vibrational levels of the alizarin S_1 state, which is repopulated within 450 fs. The subsequent $S_1 \rightarrow S_0$ transition occurs in about 160 ps. Regarding the principle of detailed balance it can be concluded that the 160 ps component of the ground-state recovery directly reflects the forward transition rate from S_1 to S_0 due to the large difference in energy of the two states. As mentioned above, population and depopulation times in general are determined by multiple forward and back-reaction channels. This usually has to be considered when the microscopic rates are derived from the experimental data.

The second reaction pathway leads to a direct ground-state recombination (without S_1 repopulation) with a dominant time constant of 2.4 ps. A few of the electrons may become localized in traps with a weak electronic coupling to the alizarin and therefore recombine very slow ($\tau > 1$ ns). The heterogeneuos nature of colloidal suspensions may be primarily responsible for the dispersive character of this reaction dynamics.

The comparison between the systems alizarin/TiO_2 and alizarin/ZrO_2 shows that in both cases an ultrafast electron injection and cation formation takes place that cannot be time-resolved with our current setup. So an upper limit for the injection time of about 100 fs can be determined in agreement with the standard electron transfer theory, predicting very fast transition times for systems with a high electronic coupling constant.

V. Conclusions

Our measurements underline the crucial role of trap states in the injection mechanism of electrons from dye molecules to semiconductor surfaces. For investigations on systems such as dye/TiO_2 it is difficult to distinguish the two steps of the electron injection: from the dye molecule to surface trap states and the subsequent injection to the conduction band of TiO_2. The first detailed studies of the system alizarin/ZrO_2 presented here investigate a system where only the first step, the electron injection into trap states, can be observed. The ultrafast time

scale of this transition ($\tau < 100$ fs) indicates the high influence of surface effects on the injection mechanism. So even if quantum size effects play a minor role considering volume effects for colloids with $r > 4$ nm (see ref 6c and references therein), the associated surface effects, especially the nature of the trap states and therewith the injection dynamics, can be affected. For this reason a defined implementation or manipulation of surface defects and trap states to influence and optimize the charge injection dynamics is thinkable. We showed that for the effective analysis of such charge injection processes visible pump/white light probe experiments represent a powerful tool because they allow us to record the excited state of the dye, its ground state, the dye cation, and the trapped electron simultaneously. This is the prerequisite for an unambiguous interpretation of the recorded data. Combined with a global fitting procedure, it is possible to directly measure population and depopulation rates of the different electronic states. Further femtosecond experiments with improved the temporal resolution down to less than 25 fs will allow the direct observation of the electron injection process for strongly coupled systems such as alizarin/TiO_2 in the near future.

Acknowledgment. The authors would like to thank W. Zinth for helpful discussions. This work is supported by the Deutsche Forschungsgemeinschaft (SFB 377/TP B10). J.E.M. and M.G. are grateful to the Swiss National Science Foundation (FNRS) for financial support.

References and Notes

(1) Wu, T.; Liu, G.; Zhao, J. *J. Phys. Chem. B* **1999**, *103*, 4862.

(2) (a) Hagfeldt, A.; Grätzel, M. *Chem. Rev.* **1995**, *95*, 49. (b) O'Regan, B.; Grätzel, M. *Nature* **1991**, *353*, 737. (c) Bach, U.; Lupo, D.; Comte, P.; Moser, J. E.; Weissörtel, F.; Salbeck, J.; Spreitzer, H.; Grätzel, M. *Nature* **1998**, *395*, 583.

(3) (a) Enea, O.; Moser, J.; Grätzel, M. *J. Electroanal. Chem.* **1989**, *259*, 59. (b) O'Regan, B.; Moser, J.; Anderson, M.; Grätzel, M. *J. Phys. Chem.* **1990**, *94*, 8720.

(4) (a) Nazeeruddin, M.; Liska, P.; Moser, J.; Vlachopoulos, N.; Grätzel, M. *Helv. Chim. Acta* **1990**, *73*, 1788. (b) Nazeeruddin, M. K.; Kay, A.; Rodicio, I.; Humphry-Baker, R.; Müller, E.; Liska, P.; Vlachopoulos, N.; Grätzel, M. *J. Am. Chem. Soc.* **1993**, *115*, 6382.

(5) Slama-Schwok, A.; Ottolenghi, M.; Avnir, D. *Nature* **1992**, *355*, 240.

(6) (a) Moser, J.; Grätzel, M. *J. Am. Chem. Soc.* **1984**, *106*, 6557. (b) Moser, J.; Grätzel, M.; Sharma, D. K.; Serpone, N. *Helv. Chim. Acta* **1985**, *24*, 1686. (c) Hilgendorff, M.; Sundström, V. *J. Phys. Chem. B* **1998**, *102*, 10505.

(7) Heimer, T. A.; Heilweil, E. J. *J. Phys. Chem. B* **1997**, *101*, 10990.

(8) Ghosh, H. N.; Asbury, J. B.; Weng, Y.; Lian, T. *J. Phys. Chem.* **1998**, *102*, 10208.

(9) Tachibana, Y.; Moser, J. E.; Grätzel, M.; Klug, D. R.; Durrant, J. R. *J. Phys. Chem.* **1996**, *100*, 20056.

(10) Ellingson, R. J.; Asbury, J. B.; Ferrere, S.; Ghosh, H. N.; Sprague, J. R.; Lian, T.; Nozik, A. J. *J. Phys. Chem. B* **1998**, *102*, 6455.

(11) Ghosh, H. N.; Asbury, J. B.; Lian, T. *J. Phys. Chem. B* **1998**, *102*, 6482.

(12) Hannappel, T.; Burfeindt, B.; Storck, W. *J. Phys. Chem. B* **1997**, *101*, 6799.

(13) Moser, J. E.; Noukakis, D.; Bach, U.; Tachibana, Y.; Klug, D. R.; Durrant, J. R.; Humphry-Baker, R.; Grätzel, M. *J. Phys. Chem. B* **1998**, *102*, 3649.

(14) Hannappel, T.; Zimmermann, C.; Meissner, B.; Burfeindt, B.; Storck, W.; Willig, F. *J. Phys. Chem. B* **1998**, *102*, 3651.

(15) Martini, I.; Hodak, J.; Hartland, G. V. *J. Chem. Phys.* **1997**, *107*, 8064.

(16) Burfeindt, B.; Hannappel, T.; Storck, W.; Willig, F. *J. Phys. Chem.* **1996**, *100*, 16463.

(17) Wachtveitl, J.; Huber, R.; Spörlein, S.; Moser, J. E.; Grätzel, M. *J. Photoenerg.* **1999**, *1*, 153.

(18) Rehm, J. M.; McLendon, G. L.; Nagasawa, Y.; Yoshihara, K.; Moser, J.; Grätzel, M. *J. Phys. Chem.* **1996**, *100*, 9577.

(19) Damrauer, N. H.; Cerullo, G.; Yeh, A.; Boussie, T. R.; Shank, C. V.; McCusker, J. K. *Science* **1997**, *275*, 54.

(20) Wienke, J.; Schaafsma, T.; Goossens, A. *J. Phys. Chem. B* **1999**, *103*, 2702.

(21) Kamat, P. V. *Prog. React. Kinet.* **1994**, *19*, 277.

(22) Argazzi, R.; Bignozzi, C. A.; Heimer, T. A.; Castellano, F. N.; Meyer, G. J. *J. Phys. Chem. B* **1997**, *101*, 2591.

(23) Martini, I.; Hodak, J. H.; Hartland, G. V. *J. Phys. Chem. B* **1998**, *102*, 607.

(24) Sengupta, A.; Jiang, B.; Mandal, K. C.; Zhang, J. Z. *J. Phys. Chem. B* **1999**, *103*, 3128.

(25) Moser, J. E.; Grätzel, M. *Chem. Phys.* **1993**, *176*, 493.

(26) (a) Huber, H.; Meyer, M.; Nägele, T.; Hartl, I.; Scheer, H.; Zinth, W.; Wachtveitl, J. *Chem. Phys.* **1995**, *197*, 297. (b) Nägele, T.; Hoche, R.; Zinth, W.; Wachtveitl, J. *Chem. Phys. Lett.* **1997**, *272*, 489.

(27) Wilhelm, T.; Piel, J.; Riedle, E. *Opt. Lett.* **1997**, *22*, 1474.

(28) (a) Dilawar, N.; Zaidi, Z. H. *Ind. J. Chem.* **1991**, *30a*, 890. (b) Matsumara, M.; Nomura, Y.; Tsubomura, H. *Bull. Chem. Soc. Jpn.* **1976**, *49*, 1409.

(29) Lyon, L. A.; Hupp, J. T. *J. Phys. Chem. B* **1999**, *103*, 4623.

(30) Duonghong, D.; Ramsden, J.; Grätzel, M.; Serpone, N.; Sharma, D. *J. Am. Chem. Soc.* **1982**, *104*, 2977.

(31) Bahnemann, D. W.; Hilgendorff, M.; Memming, R. *J. Phys. Chem. B* **1997**, *101*, 4265.

(32) Asahi, T.; Furube, A.; Masuhara, H. *Chem. Phys. Lett.* **1997**, *275*, 234.

(33) Furube, A.; Asahi, T.; Masuhara, H.; Yamashita, H.; Anpo, M. *J. Phys. Chem. B* **1999**, *103*, 3120.

(34) Solbrand, A.; Henningsson, A.; Södergren, S.; Lindström, H.; Hagfeldt, A.; Lindquist, S.-E. *J. Phys. Chem. B* **1999**, *103*, 1078.

(35) Usami, A. *Chem. Phys. Lett.* **1998**, *292*, 223.

(36) Lindström, H.; Rensmo, H.; Södergren, S.; Solbrand, A.; Lindquist, S.-E. *J. Phys. Chem.* **1996**, *100*, 3084.

(37) Cao, F.; Oskam, G.; Meyer, G. J.; Searson, P. C. *J. Phys. Chem.* **1996**, *100*, 17021.

(38) Moser, J.; Grätzel, M. *J. Am. Chem. Soc.* **1983**, *105*, 6547.

(39) Moser, J.; Punchihewa, S.; Infelta, P. P.; Grätzel, M. *Langmuir* **1991**, *7*, 3012.

(40) Moser, J. E.; Bonhôte, P.; Grätzel. M. *Coord. Chem. Rev.* **1998**, *171*, 245.

(41) Moser, J. E.; Wolf, M.; Lenzmann, F.; Grätzel, M. *Z. Phys. Chem.* **1999**, *212*, 85.

(42) Creutz, C.; Newton, M. D.; Sutin, N. *J. Photochem. Photobiol. A: Chem.* **1994**, *82*, 47.